# Sustained and Prolonged Delivery of Protein Therapeutics from Two-Dimensional Nanosilicates

Lauren M. Cross,[†] James K. Carrow,[†] Xicheng Ding,[†] Kanwar Abhay Singh,[†] and Akhilesh K. Gaharwar*[,†,‡,§]

[†]Department of Biomedical Engineering, [‡]Department of Material Sciences, and [§]Center for Remote Health and Technologies and Systems, Texas A&M University, College Station, Texas 77843, United States

ABSTRACT: We present a nanoengineered system for sustained and prolonged delivery of protein therapeutics, which has the potential to impact current orthopedic regeneration strategies. Specifically, we introduce two-dimensional nanosilicates with a high surface area and charged characteristics for delivery of active proteins for more than 30 days. The nanosilicates show high binding efficacy without altering the protein conformation and bioactivity. The released proteins are able to maintain high activity as demonstrated by enhanced differentiation of human mesenchymal stem cells at 10-fold lower concentration compared to the exogenous control. Utilizing the nanosilicates as a delivery vehicle could minimize the negative side effects observed because of the use of supraphysiological dosages of protein therapeutics for orthopedic regeneration strategies.

KEYWORDS: two-dimensional (2D) nanomaterials, therapeutic delivery, bone morphogenetic protein, transforming growth factor β, human mesenchymal stem cells (hMSCs), tissue engineering
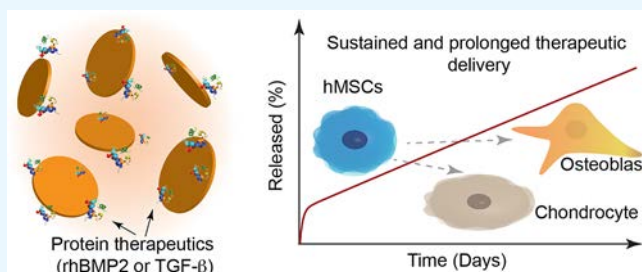
INTRODUCTION

Current clinical strategies involve the administration of inductive molecules such as recombinant human bone morphogenetic protein 2 (rhBMP2) or transforming growth factor-$\beta 3$ (TGF-β_3) to enhance tissue formation.[1,2] While successful regeneration has been observed, this is at the cost of supraphysiological doses of growth factor (1.5 mg/mL),[3] stemming from rapid clearance from the injury site and short half-lives of 7−16 min due to proteolysis in vivo.[4,5] Furthermore, growth factors like endogenous BMPs are typically found in the body at a concentration of less than 2 μg/mg.[6,7] Recent clinical studies have demonstrated significant adverse effects following the use of supraphysiological doses including heterotopic tissue formation (spatially uncontrolled tissue formation), osteolysis, and inflammation.[8−10] These adverse effects are typically attributed to poor localization and rapid release of large amounts of the growth factor.[11] Thus, there is a clinical need to develop an efficient biomolecule delivery vehicle that can result in sustained and prolonged release to reduce the effective dose toward physiological levels.

Sustained release of low concentrations of growth factor molecules would minimize the side effects of excessive dosages.[11−13] For example, sustained delivery achieved via polymeric scaffolds, micro- or nanoparticle carriers, and stimuli-responsive polymers has been explored.[14−17] However, most of these approaches result in reduction in bioactivity of entrapped therapeutic proteins.[18] In addition, many of these approaches still incorporate relatively high dosages of growth factors (micrograms−milligrams), which can be costly.[14−17]

Here, we describe a nanosilicate-based platform to minimize the concentration of delivered therapeutics, while maintaining bioactivity. Nanosilicates $(Na_{0.7}{}^{+}[(Mg_{5.5}Li_{0.3})Si_8O_{20}(OH)_4]^{-0.7}$, Laponite XLG), a two-dimensional (2D) nanomaterial, have been investigated for various biomedical applications including regenerative engineering and drug delivery.[19−22] Our recent studies have demonstrated high cytocompatibility of nanosilicates with hMSCs.[23,24] Nanosilicates readily attach to the cell membrane and are internalized by hMSCs via clathrin-mediated endocytosis.[23,25] In addition, nanosilicates have also shown to upregulate osteochondral-related genes and protein such as RUNX2, osteocalcin (OCN), aggrecan, and cartilage oligomeric matrix protein (COMP), as well as production of a mineralized matrix.[23−25]

By utilizing the nanoparticle for therapeutic delivery, it is possible to induce robust and stable differentiation of stem cells. Along with their inherent bioactivity, the disk-shaped nanosilicate particles generate a permanent negative charge on each face (via the release of Na^{+} in solution) and a positive charge along the edge (via the protonation of OH^{−} groups).[26−28] The dual charged nature of nanosilicates facilitates a wide range of possible interactions with proteins and therapeutics; importantly, these particles have previously been investigated for drug delivery applications.[20,29−32]

Specifically, cationic drugs can be immobilized by the exchangeable sodium cations of the nanosilicates.[20,30] While these previous studies have demonstrated the ability of nanosilicates to electrostatically bind proteins or small molecules, the studies do not utilize or explore the inherent bioactivity of nanosilicates. Similarly, other studies have utilized nanosilicates for growth factor delivery; however, these studies use large concentrations of the nanosilicates and deliver the growth factors via a clay gel.[33,34] No studies have investigated growth factor delivery via individual nanosilicates or demonstrated the synergistic differentiation of nanosilicate growth factor co-delivery. Recently, we have demonstrated use of nanosilicates for sequestering and prolonged delivery of pro-angiogenic therapeutics to stimulate angiogenesis.[35,36] This study demonstrated that nanosilicates is able to preserve the activity of multiple therapeutic proteins.[35,36] We will utilize the inherent bioactivity of nanosilicates and ability to sequester and delivery protein therapeutics to obtain robust differentiation of stem cells for musculoskeletal tissue engineering.

Here, we demonstrate the ability of nanosilicates to prolong the release of physiologically relevant concentrations of rhBMP2 and TGF-β_3 and synergistically contribute toward osteogenic and chondrogenic differentiation of hMSCs, respectively. We will investigate the binding efficacy of protein to the nanosilicates, and the time-dependent release of model protein from the nanosilicates. We will also evaluate the osteogenic and chondrogenic potential of the nanosilicate loaded with rhBMP2 or TGF-β_3, respectively. Utilizing the nanosilicates as a delivery vehicle could be a potential therapy to augment the inherent bioactivity of nanosilicates. In addition, nanosilicate delivery of biomolecules could reduce overall costs by reducing growth factor concentration as well as minimize the negative side effects observed in use of supraphysiological dosages for orthopedic regeneration strategies.

■ MATERIALS AND METHODS

Nanosilicate Characterization. Nanosilicates (Laponite XLG) were obtained from BYK additives. Atomic force microscopy (AFM), X-ray photoelectron spectroscopy (XPS), and attenuated total reflectance Fourier transform infrared spectroscopy (ATR–FTIR) were performed. Nanosilicate thickness was measured via AFM tapping mode (Bruker Dimension Icon Nanoscope) and analyzed with Nanoscope Analysis software. Nanosilicate chemical composition was analyzed via XPS (Omicron XPS system with Argus detector), specifically analyzing oxygen (O 1s), silicon (Si 2p), magnesium (Mg 2s, 2p), lithium (Li 1s), and sodium (Na 1s) binding energies. ATR–FTIR was performed on nanosilicate powder with a Bruker Vector 22 FTIR spectrophotometer (PIKE Technologies).

Protein/Nanosilicate Interactions. The hydrodynamic size and zeta potential of nanosilicate/protein [fetal bovine serum (FBS), Atlanta Biologicals] solutions were measured at 25 °C using Zetasizer Nano ZS (Malvern Instrument, U.K.) equipped with a He–Ne laser. Particle size was further investigated with transmission electron microscopy (TEM). The binding efficiency of nanosilicates to protein was determined using a model protein:fluorescein isothiocyanate-labeled bovine serum albumin (FITC/BSA, Sigma-Aldrich). FITC/BSA (100 μg/mL) was mixed for 1 h with various concentrations of nanosilicates (0, 1, 10, 50, 100, 500, and 1000 μg/mL) and then centrifuged to separate unbound protein. The supernatant was collected and measured using NanoDrop (495 nm excitation, 530 nm emission; NanoDrop 3300 Fluorospectrometer, Thermo Fisher Scientific) to determine binding efficiency.

In Vitro Protein Release. The release profile of protein bound to nanosilicates was determined using a model protein BSA (Sigma-Aldrich). Nanosilicate/BSA conjugates were made in phosphate

buffered serum (PBS) and mixed for 1 h to ensure binding. Samples were dialyzed (Float-A-Lyzer 100 kD MW, Spectrum) against PBS and samples were collected at various time points. The amount of released protein was quantified via a Micro BCA assay (Thermo Fisher) using standard protocol. 1-Anilinonaphthalene-8-sulfonate (ANS) assay was performed following a previously described protocol.[37] Briefly, an ANS stock solution was prepared and filtered. The stock solution concentration was then determined via an absorbance reading at 350 nm and using an extinction coefficient of 50 000 (M/cm)$^{-1}$. Protein samples were diluted and combined with ANS in a buffer of 10 mM Tris HCl, pH 7.4. Fluorescence from ANS was then measured in a plate reader at an excitation wavelength of 370 nm and an emission wavelength scan from 400 to 620 nm.

In Vitro Osteogenic Differentiation. All in vitro experiments were performed with human mesenchymal stem cells (hMSCs) passage 5 or lower, obtained from Lonza. hMSCs were cultured in osteoconductive media α-modified minimal essential media (αMEM, Hyclone), 16.5% FBS (Atlanta Biological), and 1% penicillin/streptomycin (Gibco), supplemented with 10 mM β-glycerophosphate (Sigma-Aldrich) and 50 μM ascorbic acid (BDH Chemicals). The osteogenic differentiation potential of nanosilicate/rhBMP2 (EMD-Millipore) complexes was evaluated in vitro using hMSC 2D culture. hMSCs were seeded at a density of 4000 cells/cm^2 in a 96-well plate and cultured in osteoconductive media for 7, 14, and 21 days. A negative control of untreated cells and a positive control of rhBMP2 (10 ng/mL) were used. Sample groups consisted of nanosilicates (100 μg/mL) and nanosilicate/rhBMP2 (100 μg/mL to 10 ng/mL). hMSCs were treated with nanosilicates and nanosilicate/rhBMP2 for 48 h; hMSCs treated with exogenous rhBMP2 were treated with additional rhBMP2 every media change (every 3–4 days). We did not wish to remove nanosilicates that were adhered or internalized by stem cells. To analyze osteogenic differentiation, conventional osteogenic assays were performed, specifically, alkaline phosphatase (ALP) staining and kinetic assay, alizarin red staining (ARS) and quantification of matrix mineralization, and immunostaining of osteo-specific protein OCN. Prior to staining, hMSCs were fixed with 2.5% glutaraldehyde for 15–20 min. ALP staining was performed at 7 and 14 days with NBT/BCIP 1-steps solution (nitroblue tetrazolium/5-bromo-4-chloro-3-indolyl phosphate, Thermo Fisher) for 30–60 min at room temperature. For ALP kinetic assay, cultures were incubated with ALP yellow (Sensolyte pNPP ALP assay kit, AnaSpec). ALP activity as a function of pNPP metabolism (ΔOD405) was measured using an automated plate reader and activity was normalized to DNA content (PicoGreen, Thermo Fisher). ARS (Electron Microscopy Sciences) was performed after 14 and 21 days which binds to calcium; bound ARS is proportional to the calcified matrix and was quantified by elution in acetic acid (10%), neutralized by ammonium hydroxide (10%), and spectrophotometrically measured by absorbance at 405 nm. ALP and ARS staining were visualized with a stereomicroscope (Zeiss).

For immunostaining, hMSCs were fixed (10% formalin) and then incubated in blocking solution (1% BSA in PBS) for 30 min. Samples were incubated with the primary antibody for 1 h at room temperature and then washed and incubated with a secondary antibody for 1 h. Samples were imaged with a confocal microscope (Leica TCS SP5).

For western blot analysis, hMSC protein samples were isolated via a Laemmli buffer (10% 2-mercaptoethanol, 20% glycerol, 100 mM Tris HCl, 4% SDS, and 0.2% bromophenol blue). Protein samples were separated via gel electrophoresis (Mini Gel Tank; Invitrogen) and the gel was transferred (iBlot2; Invitrogen) to a nitrocellulose membrane. BSA (5%) in PBST (0.1% Tween 20 in PBS) was used to block membranes for 30 min and then processed to investigate specific proteins (iBind; Invitrogen). β-actin, ALP, OCN, and osteopontin (OPN) primary antibodies (Thermo Fisher) and HRP-conjugated secondary antibodies (Boster Bio) were used. After incubation with antibodies according to manufacturer's protocol, membranes were developed (SuperSignal West Pico PLUS Chemiluminescent Substrate; Thermo Fisher) and imaged with LI-COR 3600 C Digit Blot Scanner and bands were quantified via LI-COR
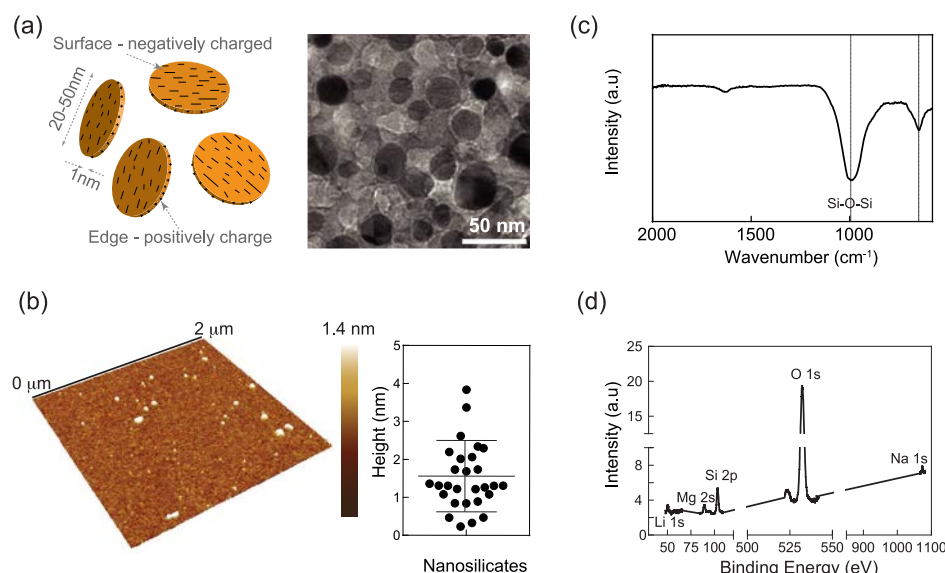
Figure 1. Physical characterization of nanosilicates. (a) TEM revealed size of 2D nanosilicates. (b) AFM indicated the thickness of nanosilicate ~1−2 nm. (c) ATR−FTIR showed characteristic peaks at ~1000 and 700 nm representing Si−O bending and stretching, respectively. (d) XPS showed chemical composition of nanosilicates as shown by the binding energies for oxygen, silicon, magnesium, lithiums and sodium.

software. Restoration and subsequent re-blocking were performed for additional protein analysis.

For quantitative reverse transcription polymerase chain reaction (qRT-PCR), RNA was isolated after 7 and 14 days of culture for spheroids and 2D seeded hMSCs, respectively. The Zymo Research Quick-RNA Miniprep Kit was utilized, following manufacture's protocol. The quality of nucleic material was measured with a spectrophotometer absorbance ratio of 280/260 nm. QuantaBio qScript cDNA SuperMix was used for cDNA synthesis following manufacture's protocol. Primers were either designed utilizing NCBI/Primer-BLAST or taken from previous literature and checked for quality via Integrated DNA Technologies' OligoAnalyzer. The following primers were designed or used: GAPDH, (forward 5′-CCTTCATTGACCTCAACTACATGG-3′, reverse 5′-TGGAA-GATGGTGATGGGATTTCC-3′), COMP (forward 5′-AA-CAGTGCCCAGGAGGAC-3′, reverse 5′-TTGTCTAC-CACCTTGTCTGC-3′), and RUNX2 (forward 5′-AGATGATGA-CACTGCCACCTCTG-3′, reverse 5′-GGGATGAAATGCTTGGGAACT-3′). For qRT-PCR, SYBR Green Reagent (Thermo Fisher) was used for amplification and samples were run and gene expression was analyzed via QuantStudio 3 Real Time PCR (Thermo Fisher) and QuantStudio and Analysis Software (Thermo Fisher), respectively.

Spheroid Culture. For spheroid culture, hMSCs were cultured in basal media and collected no later than P4. Spheroids were created through centrifugation of cell suspensions to result in 10^6 cells per spheroid for GAG quantification and 2×10^6 cells per spheroid for histology. During centrifugation (500g, 10 min), various treatments were added to media, specifically nanosilicates (50 μg/mL),[5] TGF-β_3 (Boster Bio, 10 ng/mL), or a solution of premixed nanosilicates/TGF-β_3 at equivalent concentrations. Control cells received no external treatment. Media was replaced every 3−4 days. After 21 days of culture, spheroids were washed in PBS and fixed using 10% neutral buffered formalin for 2 h. To quantify histological stains, images were processed with ImageJ software. Images were modified into an RGB grayscale stack. Color thresholding was applied equally over images within a stain cohort. Areas meeting color threshold were selected, quantified, and subsequently normalized to the total area of the spheroid. For the quantification of sulfated glycosaminoglycans (GAGs), a dimethylmethylene blue (DMMB, Sigma-Aldrich) assay was utilized. Briefly, samples were collected at day 3 and day 21. Following washing with PBS, spheroids were enzymatically digested with papain at 60 °C overnight. The dye solution was created using

DMMB (16 μg/mL), glycine (Alfa Aesar, 3.04 mg/mL), and NaCl (2.37 mg/mL) dissolved in deionized water and maintained at pH 1.5 using 0.1 M HCl. A standard curve was generated from chondroitin sulfate (Alfa Aesar).

Statistical Analysis. Plots are represented as mean and standard deviation and statistical analysis was performed using a one-way analysis of variance (ANOVA) with a Tukey's post-hoc with GraphPad Prism software. The statistical significance is presented as *P-value < 0.05, **P-value < 0.01, ***P-value < 0.001, and ****P-value < 0.0001.

■ RESULTS AND DISCUSSION

Nanosilicates (Laponite XLG) are 2D charged particles, approximately 1−2 nm thick and 25−30 nm in diameter (Figure 1a). The material properties of these nanosilicates have been extensively characterized in our previous papers.[23] Here, we investigated nanosilicate size distribution via TEM and AFM. TEM revealed uniform disk-shaped particles, and AFM images showed that nanoparticle thickness was ~1.5 nm (Figure 1a,b). Surface characteristics of nanosilicates were also evaluated via ATR−FTIR, confirming the presence of O−Si−O stretching and bending around 1000 and 700 cm^{-1}, respectively (Figure 1c).[38,39] Utilizing XPS, the presence of sodium, oxygen, silicon, magnesium, and lithium was identified, supporting chemical makeup of the nanosilicates ($Na_{0.7}^{+}[(Mg_{5.5}Li_{0.3})Si_8O_{20}(OH)_4]^{-0.7}$) (Figure 1d). In agreement with the empirical formula of nanosilicates, the XPS data support oxygen as the most prevalent ion followed by silicon. As XPS and ATR−FTIR are surface techniques and the faces of the nanosilicates have a larger surface area, these data also support the presence of silicon and oxygen on the negative face of the nanosilicates. Additionally, the presence of O−Si−O bending and stretching on the surface exposes the two-lone pair of electrons on each oxygen atom, contributing to the negative surface charge. Similarly, the positive edge of the nanosilicates stems from the protonation of OH$^-$ groups. Importantly, the negatively charged faces and positively charged edges of the nanosilicates allow for a wide range of proteins to electrostatically bind or interact with the nanoparticles.
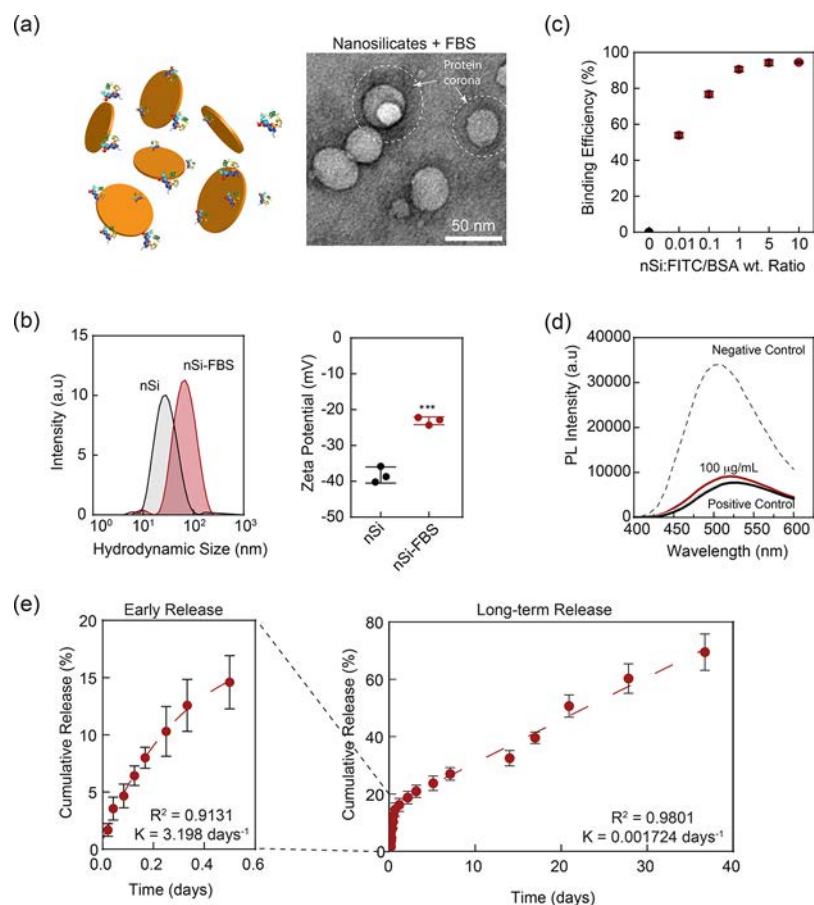
Figure 2. Nanosilicates strongly interact with proteins. (a) Schematic of protein interactions with nanosilicates. TEM images of nanosilicates in FBS solution. (b) DLS of nanosilicates (nSi) and nanosilicates with FBS (nSi−FBS) demonstrating shift in particle size with addition of protein solution. Zeta potential of nanosilicates and nanosilicates with FBS; once in contact with protein, particle charge shifts to be more positive (***P-value < 0.001). (c) Percent binding efficiency of nanosilicates to protein; nearly 100% binding was observed at a ratio of nanosilicates to protein of 5:1. (d) ANS assay demonstrating no change in protein's secondary structure when bound to nanosilicates as indicated by minimal shift in the fluorescent peak compared to completely denature protein (positive control). (e) Early and long-time release of protein from nanosilicates. Protein release was monitored for over 30 days.

When nanosilicates are introduced into a physiological environment, their interactions with proteins result in the formation of a protein corona which directs nanoparticle−cell interactions. The nanoparticle−protein complex can influence cellular transport as well as influence surface receptors and cellular pathways.[40−42] Therefore, these strong electrostatic interactions can be used to bind therapeutic growth factors and facilitate prolonged delivery. We previously determined (via whole-transcriptome sequencing) that nanosilicates trigger membrane targeting and can affect several signaling pathways related to growth factor stimulus and osteochondral-specific pathways.[23] Further gene ontological (GO) analysis has indicated that nanosilicate treatment of hMSCs results in the activation of "cellular response to growth factor stimulus," thereby conditioning the hMSC population for a growth factor treatment.[23] On the basis of this information, nanosilicates can be used to deliver therapeutics near the cell membrane or in the cytosol. For example, growth factors such as rhBMP2 or TGF-β_3 can be electrostatically bound to nanosilicates to enhance their inductive ability, thereby reducing the overall dose of the growth factor. It is expected that the combination of growth factor with bioactive nanosilicates will allow for enhanced and synergistic osteogenic and chondrogenic differentiation in hMSCs.

Nanosilicates Strongly Interact with and Sequester Proteins. The shape, size, and surface charge of a nanoparticle will influence protein corona formation and subsequently cellular interactions.[43−45] For example, the size of the nanoparticle can affect uptake mechanisms as larger particles (>0.5 μm) are often phagocytosed versus endocytosed.[44] In addition, nanoparticle shape can affect binding to the cell surface and subsequent membrane wrapping in particle uptake. Finally, nanoparticle surface charge can affect protein adsorption and bioactivity as well as particle uptake. Here, we first investigated nanosilicate/protein interactions using FBS. The dual charge of nanosilicates allows for a variety of electrostatic interactions or binding with serum proteins (Figure 2a). The size and charge of the resulting nano-silicate/FBS complexes were investigated, and TEM images revealed the presence of protein surrounding the nanosilicates in samples where FBS had been introduced. Further investigation with dynamic light scattering (DLS) confirmed this result; a significant increase in particle size was observed for the nanosilicate/protein complex (∼50 nm) compared to nanosilicates alone (∼28 nm) (Figure 2b). Similarly, unadulterated nanosilicates exhibited significant negative zeta potential (−38 ± 2 mV) compared to the putative nano-silicate/protein complexes formed in FBS (−23 ± 1 mV),
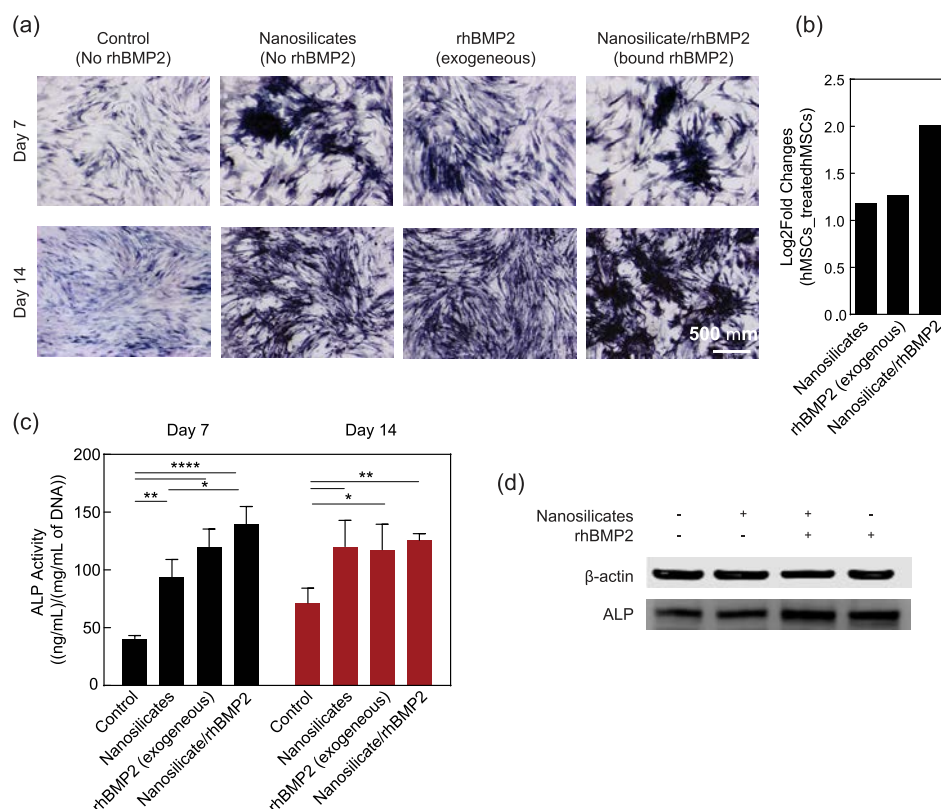
Figure 3. rhBMP2 bound to nanosilicates enhances ALP production. Nanosilicates and rhBMP2 bound to nanosilicates were delivered once while exogenous rhBMP2 was delivered every media change (every 3−4 days). (a) rhBMP2 bound to nanosilicates enhances ALP protein production compared to exogenous rhBMP2. (b) RUNX2 gene expression after 14 days. (c) ALP activity after 7 and 14 days of culture. After 7 days, rhBMP2 delivered via nanosilicates increased production significantly *P-value < 0.05, **P-value < 0.01, ****P-value < 0.0001. (d) Western blot of ALP after 14 days reveals increase in protein production for groups treated with nanosilicate bound and exogenous rhBMP2.

indicating that regions of the negatively charged faces were indeed coated with protein (Figure 2b). Importantly, while the complex's zeta potential shifted significantly compared to the nanosilicates, the value remained within the range of particle stability. A previous study investigated silica nanoparticle interactions with serum proteins and observed a similar shift in resulting particle size and zeta potential.[43] These results demonstrate that nanosilicates can strongly interact with proteins and/or therapeutic molecules. In addition, these results support our previous observation that the charged characteristic of nanosilicates strongly interact with serum protein.[23] Moreover, it is expected that the type of protein sequestered on nanosilicates will dictate cellular internalization, which is expected to be clathrin-mediated endocytosis based on our previous observation.[23]

Nanosilicates Strongly Bind and Release Proteins. Nanosilicate/protein binding efficacy and release kinetics were investigated using model proteins, specifically BSA. Utilizing a fixed concentration of BSA labeled with FITC (FITC/BSA, 100 μg/mL) and various concentrations of nanosilicates (0− 1000 μg/mL), binding efficiency of the nanosilicates was examined. Approximately 100% binding efficiency was observed for the mass ratio of nanosilicate/FITC/BSA above 5:1 (Figure 2c). This indicates that the concentration of nanosilicates must be five times greater than the concentration of protein or therapeutic to attain the most efficient binding. Previous studies also support the ability of nanosilicates to bind proteins or small molecules. For example, one study demonstrated doxorubicin simply mixed with a nanosilicate

suspension allowed for doxorubicin binding or encapsulation through ion exchange in the interlayered space of the dispersed nanosilicates.[30,46] Intriguingly, even nonionic drugs such as dexamethasone have also recently been immobilized on nanosilicates.[20]

In addition to binding efficiency, the retained structure of the bound protein or therapeutic is essential as the protein corona of the nanoparticle will direct subsequent uptake or delivery. Therefore, utilizing ANS, we assessed changes in conformation of the bound protein.[47,48] In this assay, the fluorescent dye binds to hydrophobic regions of the protein and so changes in fluorescence signal indicate a change in the exposed hydrophobic regions due to protein conformation change. No significant change in fluorescence was observed once protein was bound to the nanosilicates compared to isolated protein. This indicated a minimal effect of nanosilicate binding on the protein structure, suggesting that protein activity is retained (Figure 2d). Importantly, these results support previous studies that report negatively charged nanoparticles do not perturb the protein structure.[41]

The release of protein from nanosilicates was monitored over a course of 30 days under physiological conditions. After an initial burst release of loosely bound protein within the first 12 h, nanosilicates displayed sustained release of bound BSA (Figure 2e). The release kinetic was fit to a two-phase association model with an R^2 of 0.98, indicating a good fit for this release profile. The rate constant for long-term release was calculated as 0.001724 days^{-1}. This study supports our hypothesis that nanosilicates can be used as a vehicle for
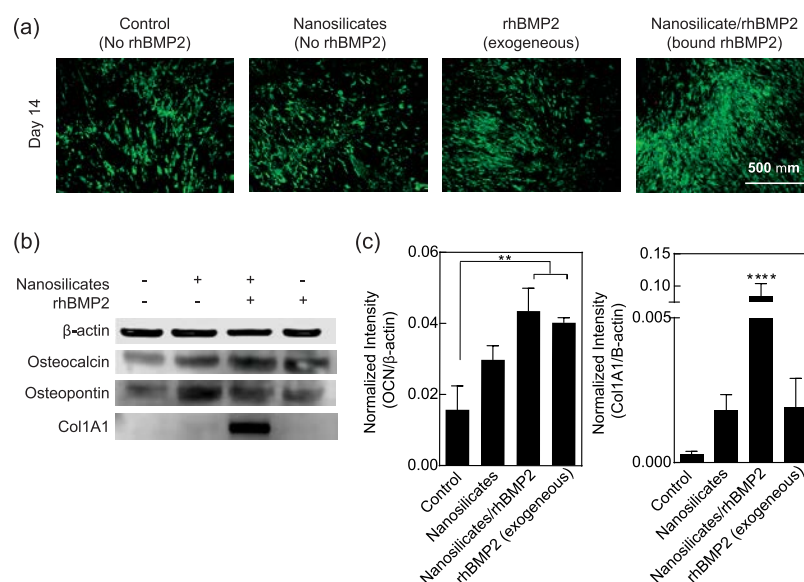
Figure 4. Sustained delivery of rhBMP2 promotes osteospecific protein production. (a) OCN production enhanced by dual delivery of nanosilicates and growth factor after 14 days of culture. (b) Western blot of OCN and OPN after 14 days revealed increase in protein production in all treatment groups compared to the control. In addition, collagen type I (Col1A1) production was increased in the nanosilicate/rhBMP2-treated hMSCs. (c) Quantification of OCN showed a significant increase in exogenous and nanosilicate/rhBMP2 groups compared to the control (**P-value < 0.01). In addition, quantification of intensity values for Col1A1 revealed a significant increase in protein production for nanosilicate/rhBMP2 (****P-value < 0.0001).

prolonged delivery of therapeutics. As 100% release was not observed, we believe that some protein may remain bound to the nanosilicates. In addition, released protein was analyzed via an ANS assay to investigate the retained protein structure. Results indicated similar shifts in florescence compared to unmodified protein, suggesting that the bioactivity of released protein was retained. These studies support the ability of nanosilicates to bind and release proteins while maintaining the protein structure.

Nanosilicate/rhBMP2 Delivery Promotes Production of Osteo-Related Proteins. The activity of released growth factor (rhBMP2) from nanosilicates was assessed using in vitro studies. Nanosilicates/rhBMP2 (100 μg/mL:10 ng/mL) were subjected to seeded hMSC and osteogenic differentiation was monitored over 4 weeks. The mass ratio of nanosilicate/growth factor is 10 000:1 to make sure that 100% of protein is sequestered on nanosilicates. We used untreated hMSCs, nanosilicate (100 μg/mL)-treated hMSCs, and exogenous rhBMP2-treated hMSCs as controls. hMSCs treated with nanosilicates/rhBMP2 and nanosilicates were treated for 48 h, after which media was changed with osteoconductive media every 3−4 days, while the exogenous rhBMP2 treated hMSCs were provided with fresh osteoconductive media containing rhBMP2 (10 ng/mL) every 3−4 days. After 7 and 14 days of culture, the production and activity of ALP (an early marker for osteogenic differentiation) were evaluated. Early on, an increase in ALP staining using NBT/BCIP and quantification was observed in hMSCs treated with nanosilicates/rhBMP2 compared to hMSCs treated with exogenous rhBMP2 (Figure 3a,c). Similarly, using qRT-PCR, Runx2, an early gene marker for osteogenic differentiation, was quantified and a significant increase in gene expression was observed in hMSCs treated with nanosilicate/rhBMP2 (Figure 3b). Additionally, a significant increase in ALP production was observed in the nanosilicate, nanosilicates/rhBMP2, and exogenous rhBMP2 groups compared to untreated controls after 7 and 14 days of

culture (Figure 3c). Similarly, ALP protein production was monitored via western blot after 14 days and an increase in protein bands was observed in the groups containing exogenous and nanosilicates/rhBMP2 (Figure 3d). Notably, the production of ALP in hMSCs treated once with nanosilicate/rhBMP2 (10 ng/mL) was comparable or greater than that of multiple treatments with exogenous rhBMP2 (20− 40 ng/mL between 7 and 14 days). This significant increase in ALP and Runx2 production with nanosilicate/rhBMP2 suggests a synergistic osteogenic response from nanosilicates and rhBMP2.

In addition, the osteospecific marker OCN, one of the most abundant noncollagenous proteins in bone,[49] was evaluated via immunostaining and western blot analysis after 14 days of culture. OCN expression was greater in the hMSCs treated with nanosilicate/rhBMP2 compared to nanosilicates or rhBMP2 alone (Figure 4a). Further quantification of protein bands for OCN revealed a significant increase in protein production for hMSCs treated with exogenous rhBMP2 and nanosilicates/rhBMP2 compared to untreated control (Figure 4b,c). OPN, which is important for biomineralization,[50] was expressed in all groups except the untreated control. A distinct band for COL1A1 was observed in nanosilicate/rhBMP2 treated hMSCs, compared to nanosilicate and exogenous rhBMP2 treated hMSCs. Further quantification of the band intensity supported the significant increase in COL1A1 production in the nanosilicate/rhBMP2 group compared to all other treatments. While previous studies have shown that addition of nanosilicates to stem cells increases COL1A1 production,[23] the significant increase in protein production with nanosilicates/rhBMP2 could have masked detection in the nanosilicate and exogenous rhBMP2 groups. Regardless, COL1A1 is very abundant in bone tissue so the increase in the protein production with treatment of both rhBMP2 and nanosilicates supports the synergistic contribution to enhance osteogenic differentiation of hMSCs.

Nanosilicate/rhBMP2 Delivery Direct Formation of Mineralized ECM by hMSCs. Finally, the one-time delivery of nanosilicates/rhBMP2 significantly increased matrix mineralization or calcium deposit compared to multiple treatments of rhBMP2 alone. ARS revealed an increase in calcium deposition from 14 and 28 days (Figure 5a). After 14 days of
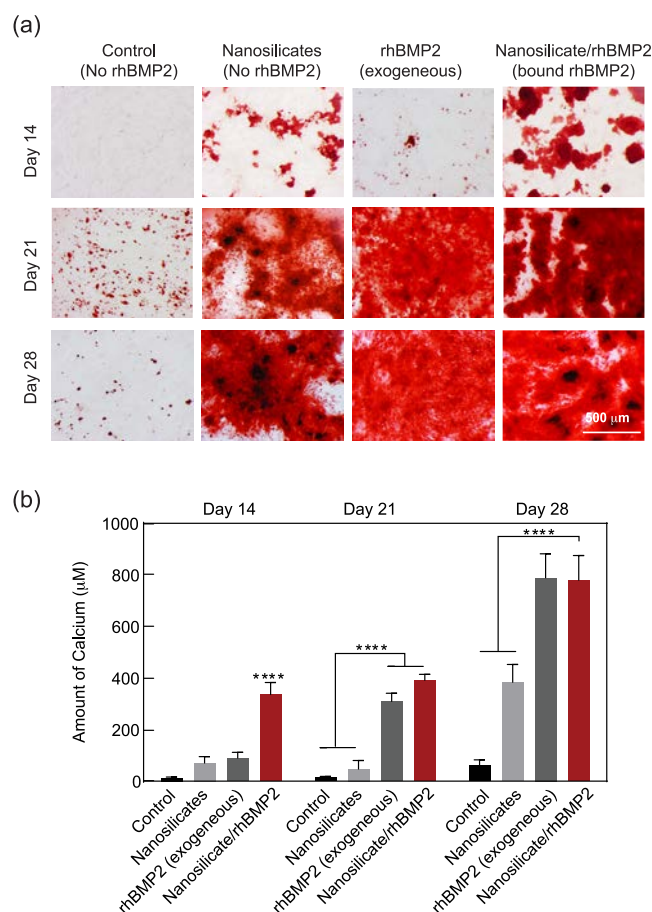

Figure 5. Sustained delivery of rhBMP2 from nanosilicates increases matrix mineralization. (a) Matrix mineralization or calcium deposit was significantly enhanced by dual delivery after 14 and 21 days compared to exogenous growth factor alone. Similarly, after 28 days, staining for mineralized matrix between exogenous rhBMP2 control and delivered rhBMP2 was comparable. (b) Quantification of calcium deposit after 14, 21, and 28 days revealed a significant increase in deposit with the delivery of rhBMP2 via nanosilicates at all time points (****P-value < 0.0001).

culture, there was evidence of the calcified matrix or bone modulus in the hMSC culture treated with nanosilicate/rhBMP2. Previous studies utilizing nanosilicates have also shown that these particles can facilitate nodule formation.[24] While increased staining for calcium deposition was observed in hMSCs treated with exogenous rhBMP2 at 21 and 28 days, these nodules were not present, suggesting that the co-delivery has a greater and synergistic effect on osteogenic differentiation. Matrix mineralization at 14, 21, and 28 days was quantified (Figure 5b). A significant increase in calcium production was observed in the nanosilicate/rhBMP2 groups across all days. At the later time points of 21 and 28 days, hMSCs treated with exogenous rhBMP2 also produced significant calcium deposits compared to control and nanosilicate-treated groups.

The observed increase in osteospecific markers and mineralized matrix production with the nanosilicate bound rhBMP2 not only supported retained rhBMP2 activity, but more importantly, this co-delivery system induced synergistic and enhanced osteogenic differentiation. In addition, the dosage of rhBMP2 (10 ng/mL) delivered with the nanosilicates was significantly less than concentrations typically administered for in vitro studies; for example, previous studies often incorporated doses greater than 100 ng/mL.[14,15,33] While previous studies have utilized nanosilicates for delivery of growth factors, these studies have encapsulated growth factors within a nanosilicate gel or used the gel to sequester exogenous growth factors rather than binding them to the individual particles.[33,34] Clay gel with encapsulated rhBMP2 displays decreased bioactivity compared to groups with clay gels sequestering exogenous rhBMP2.[33,34] In addition, previous studies merely seeded cells on top of fabricated gels, limiting cellular interactions with individual nanosilicates.[33] In the present study, nanosilicates with low dosage of rhBMP2 (10 ng/mL) were directly applied to hMSC culture; this allows hMSCs to interact with individual particles, and the rhBMP2 delivery can be localized to the cell. Importantly, this dual delivery occurred only once during the study and was only ~10% of the continual rhBMP2 treatment of the positive control. Nanosilicates interact with the cell surface via the formed protein corona and some particles are internalized as described in previous work.[23] By precoating nanosilicates with rhBMP2, nanosilicate interactions with the cell surface could be directed to the BMP surface receptors. While the exact mechanisms behind the enhanced differentiation response with the delivery of nanosilicate/rhBMP2 are still unknown, it is possible that some nanosilicates could remain attached to the cell surface and continue to deliver the growth factor. In addition, it is possible that nanosilicates can sequester growth factors released by cells and direct cell functions. Future studies will investigate these mechanisms more closely. For the present study, by reducing the concentration of rhBMP2, this dual delivery system provides an alternative and synergistic treatment for directing hMSC osteogenic differentiation and subsequently bone regeneration, minimizing both the cost and negative side effects associated with the typical high doses.

Nanosilicate/TGF-β_3 Delivery Promotes Chondrogenic Differentiation of hMSCs. To investigate the ability of nanosilicates to deliver TGF-β_3 for chondrogenic differentiation of hMSCs, we modified the culture conditions of the hMSCs. Specifically, hMSCs were placed into three-dimensional (3D) spheroids to recapitulate the cell−cell interactions found in native cartilage (Figure 6a). Similar to the previous studies, cells were cultured in the absence of growth factor unless specified otherwise. Over the course of 1 week, untreated hMSCs, hMSCs treated with nanosilicates, and hMSCs treated with exogenous TGF-β_3 displayed minimal differences regarding matrix synthesis with both sulfated GAGs (Alcian Blue) and collagens (Trichrome). Interestingly, the delivery of TGF-β_3 bound to nanosilicates appeared to improve chondrogenic behavior as early as 3 days from total GAGs quantification (Figure 6b) and 7 days from GAGs and collagen staining (Figure 6c,d) following spheroid formation. At later culture times (21 days) to indicate successful induction into a cartilage phenotype, histology was performed to monitor matrix component synthesis (Figure 6c,d). Alcian Blue stains indicated an increase in sulfated GAG production within the spheroid. Quantification of this staining through color
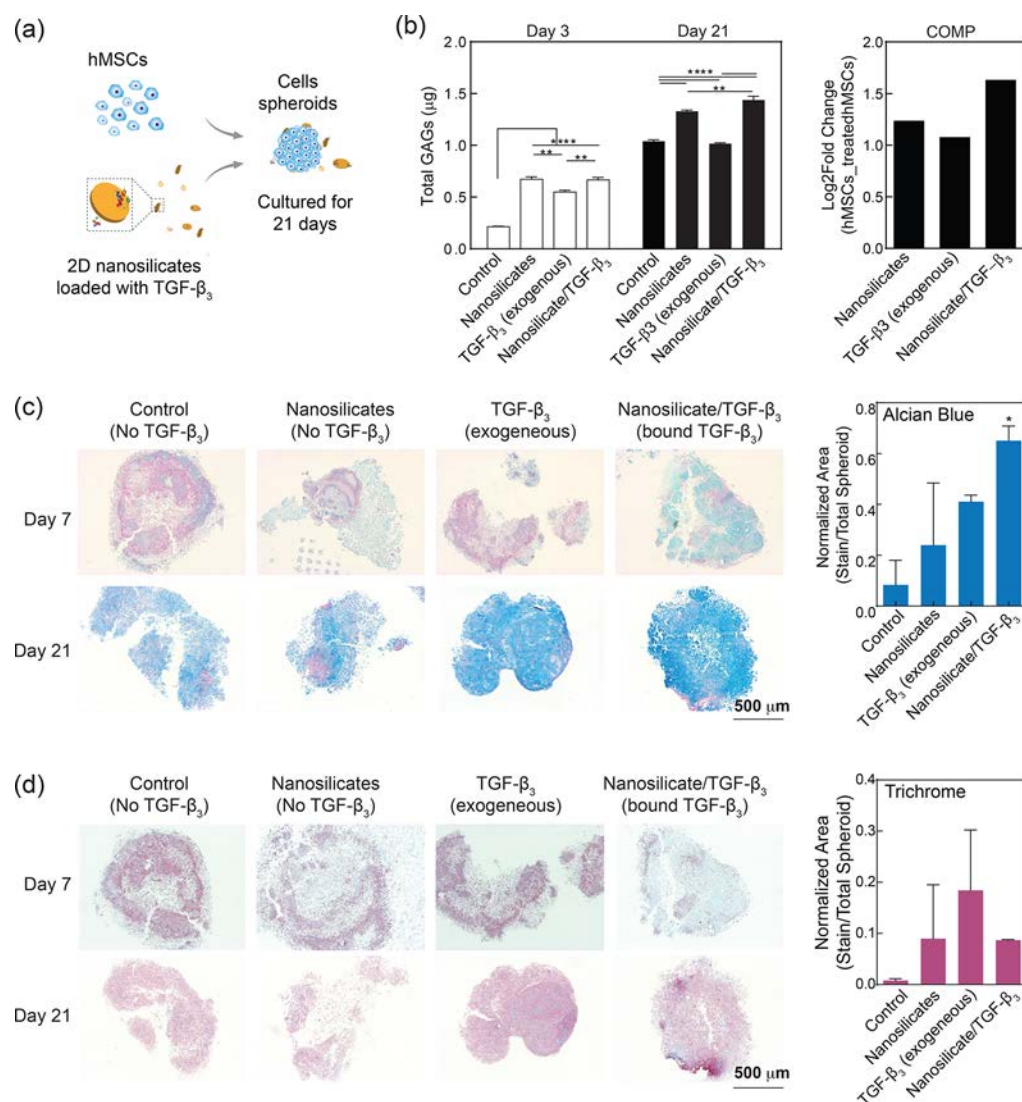
Figure 6. Sustained delivery of TGF-β_3 from nanosilicates increases production of cartilage-related ECM. (a) Spheroid from hMSCs treated with nanosilicate-loaded TGF-β_3 was obtained ad cultured for 21 days. (b) Significant increase in total GAGs was observed because of nanosilicate treatment, nanosilicate/TGF-β_3, and exogenous TGF-β_3 compared to untreated control. COMP was upregulated in the nanosilicate/TGF-β_3 group compared to control. Histology images and quantification using (c) Alcian Blue (GAGs) and (d) Trichrome (collagen) indicate that released TGF-β_3 from nanosilicates have similar activity compared exogenous TGF-β_3 (*P-value < 0.05).

thresholding in image software ImageJ revealed a significant increase in matrix production for spheroids with nanosilicate/TGF-β_3 delivery. While continuous delivery of TGF-β_3 alone increased production of a cartilage-specific matrix, the co-treatment of nanosilicates with TGF-β_3 provided the greatest stimulation toward the chondro phenotype at 10-fold lower concentration of TGF-β_3. In addition, using qRT-PCR, COMP expression was monitored after 7 days (Figure 6b). hMSCs treated with nanosilicates and exogenous TGF-β_3 exhibited similar expression profiles, whereas hMSCs treated with the co-delivery of nanosilicate/TGF-β_3 had greater COMP expression. This study supports our previous work in which we demonstrated an increased cartilage-specific gene because of nanosilicate treatment alone.[23] From our previous work utilizing whole-transcriptome sequencing, we also observed that nanosilicates activated pathways related to TGF-β family proteins (e.g., response to transforming growth factor β, GO:0071559), which further strengthen the current work.[23]

Our nanosilicate/growth factor delivery system exhibits great promise for future orthopedic regeneration strategies. To assist in localization in vivo, the system could easily be incorporated into various tissue engineering constructs, including prefabricated scaffolds currently utilized to deliver therapeutics, like collagen sponge or gel putty. Incorporation of nanosilicates with collagen sponge or putty can prolong the delivery of entrapped factors and thus reduce the overall concentration. Importantly, collagen sponges are already used in clinical practice for bone regeneration, so incorporation of this nanosilicate/growth factor system into a pre-established material could expedite clinical translation. Moreover, nanosilicates can also be combined with various ranges of natural and synthetic polymeric hydrogel systems including gelatin,[19,51] kappa carrageenan,[36,52] and poly(ethylene oxide)[53] for sustained and prolonged delivery of therapeutic proteins. These nanocomposite systems have been investigated for both injectable systems[54] and 3D printed constructs.[29,55,56] By localizing and patterning therapeutic protein, regionalized

differentiation of stem cells on gradient scaffolds can be obtained to mimic the osteochondral interface.[57] Moreover, this technology can be extended to load-bearing applications by using in conjunction with an interbody fusion cage or by combining nanosilicates with biodegradable implants made from poly(propylene fumarate) or poly(L-lactic acid) or poly(caprolactone).

CONCLUSIONS

Our nanosilicate-based platform demonstrates the potential for superior orthopedic tissue engineering by reducing the required dose of growth factors. Because of the dual-charged and disc-shaped characteristics of nanosilicates, the particles can electrostatically bind and subsequently release therapeutic proteins such as rhBMP2 or TGF-β_3 over a prolonged duration. The nanosilicates also show high binding capabilities without altering protein conformation. The released proteins were able to maintain high efficacy as demonstrated by in vitro experiments. Enhanced osteochondral differentiation in hMSCs at a lower concentration (10 ng/mL) was observed compared to exogenous control. Overall, this platform could be easily modified and applied to future biomedical applications requiring sustained therapeutic delivery, for example, orthopedic tissue engineering.

AUTHOR INFORMATION

Corresponding Author
*E-mail: gaharwar@tamu.edu. Phone: 979-458-5540. Fax: 979-845-4450.

ORCID
Akhilesh K. Gaharwar: 0000-0002-0284-0201

Author Contributions
L.M.C., J.K.C., and A.K.G. designed research; L.M.C. and J.K.C. performed nanoparticles characterization and in vitro studies, X.D. performed qRT-PCR on spheroid samples, and K.A.S performed ANS assay. The manuscript was written through contributions of all authors. All authors have given approval to the final version of the manuscript.

Notes
The authors declare no competing financial interest.

ACKNOWLEDGMENTS

REFERENCES

(1) Lanza, R.; Atala, A. *Essentials of Stem Cell Biology*; Elsevier Science, 2013.

(2) Ronga, M.; Fagetti, A.; Canton, G.; Paiusco, E.; Surace, M. F.; Cherubino, P. Clinical applications of growth factors in bone injuries: experience with BMPs. *Injury* **2013**, *44*, S34−S39.

(3) Administration., F. U. S. F. a. D. InFUSE Bone Graft/LT-CAGE Lumbar Tapered Fusion Device. https://www.accessdata.fda.gov/cdrh_docs/pdf/p000058b.pdf, accessed 10 Jan 2019.

(4) Zhang, Q.; He, Q.-F.; Zhang, T.-H.; Yu, X.-L.; Liu, Q.; Deng, F.-l. Improvement in the delivery system of bone morphogenetic protein-2: a new approach to promote bone formation. *Biomed. Mater.* **2012**, *7*, 045002.

(5) Lee, K.; Silva, E. A.; Mooney, D. J. Growth factor delivery-based tissue engineering: general approaches and a review of recent developments. *J. R. Soc., Interface* **2011**, *8*, 153−170.

(6) Prolo, D. J.; Rodrigo, J. J. Contemporary bone graft physiology and surgery. *Clin. Orthop. Relat. Res.* **1985**, *200*, 322−342.

(7) Ríos, D. L.; López, C.; Álvarez, M. E.; Samudio, I. J.; Carmona, J. U. Effects over time of two platelet gel supernatants on growth factor, cytokine and hyaluronan concentrations in normal synovial membrane explants challenged with lipopolysaccharide. *BMC Musculoskeletal Disord.* **2015**, *16*, 153.

(8) Ong, K. L.; Villarraga, M. L.; Lau, E.; Carreon, L. Y.; Kurtz, S. M.; Glassman, S. D. Off-Label Use of Bone Morphogenetic Proteins in the United States Using Administrative Data. *Spine* **2010**, *35*, 1794−1800.

(9) Carragee, E. J.; Hurwitz, E. L.; Weiner, B. K. A critical review of recombinant human bone morphogenetic protein-2 trials in spinal surgery: emerging safety concerns and lessons learned. *Spine J.* **2011**, *11*, 471−491.

(10) Lad, S. P.; Nathan, J. K.; Boakye, M. Trends in the use of bone morphogenetic protein as a substitute to autologous iliac crest bone grafting for spinal fusion procedures in the United States. *Spine* **2011**, *36*, E274−E281.

(11) Shields, L. B. E.; Raque, G. H.; Glassman, S. D.; Campbell, M.; Vitaz, T.; Harpring, J.; Shields, C. B. Adverse effects associated with high-dose recombinant human bone morphogenetic protein-2 use in anterior cervical spine fusion. *Spine* **2006**, *31*, 542−547.

(12) Winn, S. R.; Uludag, H.; Hollinger, J. O. Sustained release emphasizing recombinant human bone morphogenetic protein-2. *Adv. Drug Delivery Rev.* **1998**, *31*, 303−318.

(13) Quinlan, E.; Thompson, E. M.; Matsiko, A.; O'Brien, F. J.; López-Noriega, A. Long-term controlled delivery of rhBMP-2 from collagen-hydroxyapatite scaffolds for superior bone tissue regeneration. *J. Controlled Release* **2015**, *207*, 112−119.

(14) Samorezov, J. E.; Headley, E. B.; Everett, C. R.; Alsberg, E. Sustained presentation of BMP-2 enhances osteogenic differentiation of human adipose-derived stem cells in gelatin hydrogels. *J. Biomed. Mater. Res., Part A* **2016**, *104*, 1387−1397.

(15) Seo, B.-B.; Choi, H.; Koh, J.-T.; Song, S.-C. Sustained BMP-2 delivery and injectable bone regeneration using thermosensitive polymeric nanoparticle hydrogel bearing dual interactions with BMP-2. *J. Controlled Release* **2015**, *209*, 67−76.

(16) Bastami, F.; Paknejad, Z.; Jafari, M.; Salehi, M.; Rezai Rad, M.; Khojasteh, A. Fabrication of a three-dimensional β-tricalcium-phosphate/gelatin containing chitosan-based nanoparticles for sustained release of bone morphogenetic protein-2: Implication for bone tissue engineering. *Mater. Sci. Eng., C* **2017**, *72*, 481−491.

(17) Vo, T. N.; Kasper, F. K.; Mikos, A. G. Strategies for controlled delivery of growth factors and cells for bone regeneration. *Adv. Drug Delivery Rev.* **2012**, *64*, 1292−1309.

(18) Yu, X.; Suárez-González, D.; Khalil, A. S.; Murphy, W. L. How does the pathophysiological context influence delivery of bone growth factors? *Adv. Drug Delivery Rev.* **2015**, *84*, 68−84.

(19) Xavier, J. R.; Thakur, T.; Desai, P.; Jaiswal, M. K.; Sears, N.; Cosgriff-Hernandez, E.; Kaunas, R.; Gaharwar, A. K. Bioactive nanoengineered hydrogels for bone tissue engineering: a growth-factor-free approach. *ACS Nano* **2015**, *9*, 3109−3118.

(20) Fraile, J. M.; Garcia-Martin, E.; Gil, C.; Mayoral, J. A.; Pablo, L. E.; Polo, V.; Prieto, E.; Vispe, E. Laponite as carrier for controlled in vitro delivery of dexamethasone in vitreous humor models. *Eur. J. Pharm. Biopharm.* **2016**, *108*, 83−90.

(21) Mousa, M.; Evans, N. D.; Oreffo, R. O. C.; Dawson, J. I. Clay nanoparticles for regenerative medicine and biomaterial design: A review of clay bioactivity. *Biomaterials* **2018**, *159*, 204−214.

(22) Chimene, D.; Alge, D. L.; Gaharwar, A. K. Two-Dimensional Nanomaterials for Biomedical Applications: Emerging Trends and Future Prospects. *Adv. Mater.* **2015**, *27*, 7261−7284.

(23) Carrow, J. K.; Cross, L. M.; Reese, R. W.; Jaiswal, M. K.; Gregory, C. A.; Kaunas, R.; Singh, I.; Gaharwar, A. K. Widespread changes in transcriptome profile of human mesenchymal stem cells induced by two-dimensional nanosilicates. *Proc. Natl. Acad. Sci. U.S.A.* **2018**, *115*, E3905−E3913.

(24) Gaharwar, A. K.; Mihaila, S. M.; Swami, A.; Patel, A.; Sant, S.; Reis, R. L.; Marques, A. P.; Gomes, M. E.; Khademhosseini, A. Bioactive Silicate Nanoplatelets for Osteogenic Differentiation of Human Mesenchymal Stem Cells. *Adv. Mater.* **2013**, *25*, 3329−3336.

(25) Mihaila, S. M.; Gaharwar, A. K.; Reis, R. L.; Khademhosseini, A.; Marques, A. P.; Gomes, M. E. The osteogenic differentiation of SSEA-4 sub-population of human adipose derived stem cells using silicate nanoplatelets. *Biomaterials* **2014**, *35*, 9087−9099.

(26) Thompson, D. W.; Butterworth, J. T. The Nature of Laponite and Its Aqueous Dispersions. *J. Colloid Interface Sci.* **1992**, *151*, 236−243.

(27) Jatav, S.; Joshi, Y. M. Chemical stability of Laponite in aqueous media. *Appl. Clay Sci.* **2014**, *97-98*, 72−77.

(28) Ruzicka, B.; Zaccarelli, E. A fresh look at the Laponite phase diagram. *Soft Matter* **2011**, *7*, 1268−1286.

(29) Peak, C. W.; Stein, J.; Gold, K. A.; Gaharwar, A. K. Nanoengineered Colloidal Inks for 3D Bioprinting. *Langmuir* **2017**, *34*, 917−925.

(30) Wang, S.; Wu, Y.; Guo, R.; Huang, Y.; Wen, S.; Shen, M.; Wang, J.; Shi, X. Laponite nanodisks as an efficient platform for Doxorubicin delivery to cancer cells. *Langmuir* **2013**, *29*, 5030−5036.

(31) Lokhande, G.; Carrow, J. K.; Thakur, T.; Xavier, J. R.; Parani, M.; Bayless, K. J.; Gaharwar, A. K. Nanoengineered injectable hydrogels for wound healing application. *Acta Biomater.* **2018**, *70*, 35−47.

(32) Li, K.; Wang, S.; Wen, S.; Tang, Y.; Li, J.; Shi, X.; Zhao, Q. Enhanced in vivo antitumor efficacy of doxorubicin encapsulated within laponite nanodisks. *ACS Appl. Mater. Interfaces* **2014**, *6*, 12328−12334.

(33) Gibbs, D. M. R.; Black, C. R. M.; Hulsart-Billstrom, G.; Shi, P.; Scarpa, E.; Oreffo, R. O. C.; Dawson, J. I. Bone induction at physiological doses of BMP through localization by clay nanoparticle gels. *Biomaterials* **2016**, *99*, 16−23.

(34) Dawson, J. I.; Kanczler, J. M.; Yang, X. B.; Attard, G. S.; Oreffo, R. O. C. Clay gels for the delivery of regenerative microenvironments. *Adv. Mater.* **2011**, *23*, 3304−3308.

(35) Howell, D. W.; Peak, C. W.; Bayless, K. J.; Gaharwar, A. K. 2D Nanosilicates Loaded with Proangiogenic Factors Stimulate Endothelial Sprouting. *Adv. Biosyst.* **2018**, *2*, 1800092.

(36) Lokhande, G.; Carrow, J. K.; Thakur, T.; Xavier, J. R.; Parani, M.; Bayless, K. J.; Gaharwar, A. K. Nanoengineered injectable hydrogels for wound healing application. *Acta Biomater* **2018**, *70*, 35.

(37) Sikkink, L. A.; Ramirez-Alvarado, M. Biochemical and aggregation analysis of Bence Jones proteins from different light chain diseases. *Amyloid* **2008**, *15*, 29−39.

(38) Skelton, S.; Bostwick, M.; O'Connor, K.; Konst, S.; Casey, S.; Lee, B. P. Biomimetic adhesive containing nanocomposite hydrogel with enhanced materials properties. *Soft Matter* **2013**, *9*, 3825−3833.

(39) Ghadiri, M.; Hau, H.; Chrzanowski, W.; Agus, H.; Rohanizadeh, R. Laponite clay as a carrier for in situ delivery of tetracycline. *RSC Adv.* **2013**, *3*, 20193−20201.

(40) Nel, A. E.; Mädler, L.; Velegol, D.; Xia, T.; Hoek, E. M. V.; Somasundaran, P.; Klaessig, F.; Castranova, V.; Thompson, M. Understanding biophysicochemical interactions at the nano-bio interface. *Nat. Mater.* **2009**, *8*, 543−557.

(41) Fleischer, C. C.; Payne, C. K. Nanoparticle-cell interactions: molecular structure of the protein corona and cellular outcomes. *Acc. Chem. Res.* **2014**, *47*, 2651−2659.

(42) Lynch, I.; Dawson, K. A. Protein-nanoparticle interactions. *Nano Today* **2008**, *3*, 40−47.

(43) Saikia, J.; Yazdimamaghani, M.; Hadipour Moghaddam, S. P.; Ghandehari, H. Differential Protein Adsorption and Cellular Uptake of Silica Nanoparticles Based on Size and Porosity. *ACS Appl. Mater. Interfaces* **2016**, *8*, 34820−34832.

(44) Nel, A. E.; Mädler, L.; Velegol, D.; Xia, T.; Hoek, E. M. V.; Somasundaran, P.; Klaessig, F.; Castranova, V.; Thompson, M. Understanding biophysicochemical interactions at the nano-bio interface. *Nat. Mater.* **2009**, *8*, 543−557.

(45) Verma, A.; Stellacci, F. Effect of Surface Properties on Nanoparticle−Cell Interactions. *Small* **2010**, *6*, 12−21.

(46) Takahashi, T.; Yamada, Y.; Kataoka, K.; Nagasaki, Y. Preparation of a novel PEG-clay hybrid as a DDS material: dispersion stability and sustained release profiles. *J. Controlled Release* **2005**, *107*, 408−416.

(47) Hawe, A.; Sutter, M.; Jiskoot, W. Extrinsic fluorescent dyes as tools for protein characterization. *Pharm. Res.* **2008**, *25*, 1487−1499.

(48) Stryer, L. The interaction of a naphthalene dye with apomyoglobin and apohemoglobin. *J. Mol. Biol.* **1965**, *13*, 482−495.

(49) Hauschka, P. V.; Lian, J. B.; Cole, D. E.; Gundberg, C. M. Osteocalcin and matrix Gla protein: vitamin K-dependent proteins in bone. *Physiol. Rev.* **1989**, *69*, 990−1047.

(50) Denhardt, D. T.; Noda, M. Osteopontin expression and function: role in bone remodeling. *J. Cell. Biochem.* **1998**, *72*, 92−102.

(51) Paul, A.; Manoharan, V.; Krafft, D.; Assmann, A.; Uquillas, J. A.; Shin, S. R.; Hasan, A.; Hussain, M. A.; Memic, A.; Gaharwar, A. K. Nanoengineered biomimetic hydrogels for guiding human stem cell osteogenesis in three dimensional microenvironments. *J. Mater. Chem. B* **2016**, *4*, 3544−3554.

(52) Thakur, A.; Jaiswal, M. K.; Peak, C. W.; Carrow, J. K.; Gentry, J.; Dolatshahi-Pirouz, A.; Gaharwar, A. K. Injectable Shear-thinning Nanoengineered Hydrogels for Stem Cell Delivery. *Nanoscale* **2016**, *8*, 12362−12372.

(53) Peak, C. W.; Stein, J.; Gold, K. A.; Gaharwar, A. K. Nanoengineered Colloidal Inks for 3D Bioprinting. *Langmuir* **2017**, *34*, 917.

(54) Gaharwar, A. K.; Avery, R. K.; Assmann, A.; Paul, A.; McKinley, G. H.; Khademhosseini, A.; Olsen, B. D. Shear-thinning nanocomposite hydrogels for the treatment of hemorrhage. *ACS Nano* **2014**, *8*, 9833−9842.

(55) Wilson, S. A.; Cross, L. M.; Peak, C. W.; Gaharwar, A. K. Shear-Thinning and Thermo-Reversible Nanoengineered Inks for 3D Bioprinting. *ACS Appl. Mater. Interfaces* **2017**, *9*, 43449−43458.

(56) Chimene, D.; Peak, C. W.; Gentry, J. L.; Carrow, J. K.; Cross, L. M.; Mondragon, E.; Cardoso, G. B.; Kaunas, R.; Gaharwar, A. K. Nanoengineered Ionic-Covalent Entanglement (NICE) Bioinks for 3D Bioprinting. *ACS Appl. Mater. Interfaces* **2018**, *10*, 9957.

(57) Cross, L. M.; Shah, K.; Palani, S.; Peak, C. W.; Gaharwar, A. K. Gradient nanocomposite hydrogels for interface tissue engineering. *Nanomedicine* **2018**, *14*, 2465−2474.